Inorganic Chemistry

Article

pubs.acs.org/IC

Highly Active Subnanometer Au Particles Supported on TiO_2 for Photocatalytic Hydrogen Evolution from a Well-Defined Organogold Precursor, $[Au_5(mesityl)_5]$

Georges Siddiqi, Victor Mougel, and Christophe Copéret*

Department of Chemistry and Applied Biosciences, ETH-Zürich, Vladimir Prelog Weg 1-5, CH-8093 Zürich, Switzerland

Supporting Information

ABSTRACT: A highly efficient H_2 evolution photocatalyst based on TiO_2 supported subnanometer Au particles was developed on the basis of the reaction of a gold(I) molecular precursor $[Au_5Mes_5]$ (Mes = 2,4,6-trimethylphenyl), with titanium dioxide partially dehydroxylated at 120 °C. IR, UV−vis, elemental analysis, XANES, and STEM-EDX show that the deposition of $[Au_5Mes_5]$ onto TiO_2 leads to the formation of both subnanometer Au particles and chemisorbed $[Au_5Mes_5]$. The remaining organic ligands are removed via a mild treatment under H_2, yielding subnanometer gold(0) particles. A range of Au loadings (0.3, 0.9, 2.4 wt %) with similar particle sizes (<1 nm) on TiO_2 are obtained and tested in methanol-assisted photocatalytic hydrogen production under UV light. These catalysts display significantly higher activity than a commercial reference Au-TiO_2 catalyst. The presence of chemisorbed $[Au_5Mes_5]$ in the as-synthesized catalyst further improved activity, albeit at the expense of stability. This work demonstrates a simple synthetic route to obtain subnanometer Au particles on TiO_2 that display exceptional activity in photocatalysis.

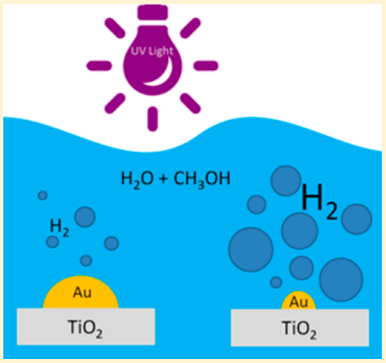

INTRODUCTION

Photocatalytic hydrogen production offers a sustainable energy source via the direct conversion of sunlight into chemical energy. First reported in 1972 using a TiO_2 single crystal anode to photoelectrochemically split water,[1] this class of catalytic systems has been extensively studied since.[2−5] Materials such as TiO_2, $SrTiO_3$, and Ta_3N_5 as well as many other combinations of mixed oxides and dopants have been developed to capture either the UV or visible spectrum of sunlight by tuning the bandgap of the material.[6−14] However, analogously to solar cells, the primary factor limiting the efficiency of these semiconductors is electron−hole recombination.[15,16] This can be mitigated by dispersing a metal cocatalyst onto the semiconductor surface to spatially separate the electrons from the holes,[7] greatly increasing photocatalytic activity.[13,15,17−22] Current research is focused both on the synthesis and performance of novel semiconductors to capture light, as well as on improving photocatalysis by tuning the metal cocatalyst.[10,23−28]

Noble metals such as Pt and Au are the most common metal cocatalysts, significantly improving hydrogen production by facilitating the separation of electrons from the holes.[5,14,29] Although the photocatalytic performance of Pt can be slightly better than Au,[30] Au boasts several notable benefits: it makes the reverse reaction of $2H_2 + O_2 \rightarrow 2H_2O$ less favorable,[31,32] and Au itself can generate electrons via plasmon resonance.[33−37] Furthermore, recent studies have also found that Au-TiO_2 can be more active than Pt-TiO_2.[38] However, Au bears several synthetic challenges, in particular the greater difficulty to control particle size and distribution by comparison to Pt cocatalysts.[29,30,39−46] Furthermore, there is no consensus on the effect of Au particle size on photocatalytic activity. While studies investigating the energetics of charge transfer across the metal semiconductor interface have indicated the benefits of decreasing Au particle,[17,47,48] others have claimed that very small Au nanoparticles are detrimental to photocatalytic performance.[19,30,31,49]

Here, we develop a robust method to generate subnanometer Au particles supported on TiO_2 via the reaction of a gold(I) organometallic precursor $[Au_5Mes_5]$ (Mes = 2,4,6-trimethylphenyl),[50] with partially dehydroxylated TiO_2 followed by a treatment under H_2. To demonstrate the potential of subnanometer Au for photocatalysis, we study the photocatalytic H_2 production from water and a CH_3OH/H_2O mixture.

EXPERIMENTAL SECTION

General Procedures. All experiments were carried out under an inert atmosphere of argon using standard Schlenk techniques or using high vacuum (10^{-5} mbar) techniques. Tetrahydrofuran (THF) was distilled from purple Na/benzophenone ketyl under Ar and stored over activated molecular sieves; toluene was dried by passage through two columns of activated alumina and degassed prior to use. H_2 was purified over R3-11 BASF catalyst/MS 4 Å prior to use. $[Au_5Mes_5]$ and reference materials (Au nanoparticles supported on SiO_2) for XANES analysis were synthesized as previous reported.[50] $[Au_5Mes_5]$ was synthesized in 55% yield via the addition of 2 equivalent of MesMgBr to a THF solution of $AuCl_3$, followed by purification and

Received: February 10, 2016

DOI: 10.1021/acs.inorgchem.6b00341
Inorg. Chem. XXXX, XXX, XXX−XXX

recrystallization.[50] The 1 wt % Au supported on P25 reference catalyst, AUROlite Au/TiO_2, from Project AuTek was purchased from Strem Chemicals. The sample is stored in a glovebox at −40 °C under Ar atmosphere, ground in an agate mortar and pestle, and weighed in Ar atmosphere before use.

Catalyst Characterization. TEM images were collected with a Philips CM12 transmission electron microscope. STEM-EDX analysis was conducted on a Tecnai F30 STEM. Samples were exposed to air for only a short time (<10 min) prior to insertion into the microscope. IR measurements were performed using a Bruker Alpha-T FTIR spectrometer inside an Ar filled glovebox. Samples were pressed into self-supporting disks using a manual press. Elemental analyses were performed by the Mikroanalytisches Labor Pascher; Remagen, Germany. NMR spectroscopy was conducted using 200 and 250 MHz Bruker spectrometers. Nitrogen adsorption experiments were performed on a BELsorp-mini II. UV−vis was acquired on a Cary 5000 UV−vis−NIR spectrometer. X-ray absorption spectroscopy (XAS) measurements at Au L_{III}-edge were performed at the SuperXAS beamline at the Swiss Light Source (Paul Scherrer Institute, Villigen, Switzerland). The SLS is a third generation synchrotron, which operates under top up mode, 2.4 GeV electron energy, and a current of 400 mA. The SuperXAS beamline is positioned on one of three superbent ports. The incident beam was collimated by Si-coated mirror at 2.8 mrad, monochromatized using a double crystal Si(111) monochromator, and focused with Rh coated toroidal mirror (at 2.8 mrad) down to 100 × 100 μm^2. The beam intensity was of 4−5 × 10^{11} ph/s. We calibrated the beamline energy using Au reference foil. We used ion chambers filled with He−N_2 gas mixtures for XAS detection in transmission. To avoid contact with air, all samples were sealed in a glovebox. Each pellet of sample (with optimized thickness for transmission detection) was placed in two aluminized plastic bags (polyaniline (15 μm), polyethylene (15 μm), Al (12 μm), polyethylene (75 μm) from Gruber-Folien GmbH & Co. KG) using an impulse sealer inside a glovebox; one sealing layer was removed just before the measurements. Powder samples for fluorescence detection were sealed in quartz capillaries (0.01 mm wall thickness, 0.9 mm outer diameter, Hilgenberg GmbH) in a glovebox using vacuum grease (Apiezon Products) and wax, and stored in sealed glass tubes under argon that were opened just before the measurements. Au(0)-SiO_2 and **1** were sealed in pellets, but due to difficulties of pressing pellets with the molecular precursor [Au_5Mes_5], this was placed in a quartz capillary. We collected XANES data in transmission mode at 298 K.

Preparation of $TiO_{2\text{-}(120)}$. TiO_2 is obtained from Evonik (P25, mixture of anatase and rutile, 60 m^2/g). Prior to deposition, P25 is calcined in a quartz reactor in a flow of synthetic air at 450 °C for 16 h (5 °C/min). After calcination the reactor is sealed while hot, cooled to room temperature under static atmosphere, and then evacuated for 20 min under high vacuum (<10^{-5} mbar). The calcined P25 is then exposed to vapor pressure of water for 30 min. Following hydration, the P25 is evacuated at room temperature for 1 h, followed by a thermal treatment under high vacuum for 16 h at 120 °C (5 °C/min temperature ramp). This P25 sample is referred to as $TiO_{2\text{-}(120)}$.

Au-TiO_2 Nanoparticle Deposition. *Preparation of* ***1****.* A yellow solution of an excess of [Au_5Mes_5] (76 mg, 0.08 mmol [Au_5Mes_5]/g TiO_2) in toluene (20 mL) was contacted with $TiO_{2\text{-}(120)}$ (613 mg) at room temperature. The suspension was stirred for 4 h, during which time the solid turned gray and the solution became paler yellow. After 4 h the filtrate was separated from the solid, which was washed with fresh toluene (3 × 20 mL), leaving a yellow filtrate after the last washing. Approximately 0.03 mmol of [Au_5Mes_5] is noted by ^{1}H NMR to remain in the filtrate after rinsing. Volatiles were evacuated *in vacuo* (10^{-2} mbar), and the solid was further dried for 3 h under high vacuum (10^{-5} mbar) to afford **1**. After drying the catalyst is stored under an inert Ar atmosphere in absence of light at −40 °C.

Preparation of ***2****.* A yellow solution of [Au_5Mes_5] (8.1 mg, 0.01 mmol [Au_5Mes_5]/g TiO_2) in toluene (20 mL) was put in contact with $TiO_{2\text{-}(120)}$ (480 mg) at room temperature. The suspension was stirred for 4 h, during which time the solid turned gray and the solution colorless. After 4 h the filtrate was separated from the solid, which was washed with fresh toluene (3 × 20 mL), leaving a colorless filtrate after the last washing. Volatiles were evacuated *in vacuo* (10^{-2} mbar), and the solid was further dried for 3 h under high vacuum (10^{-5} mbar) to afford **2**. After drying the catalyst is stored under an inert Ar atmosphere in absence of light at −40 °C.

Preparation of ***3****.* The material **3** was synthesized in a manner identical to that of **2**, except the amount of [Au_5Mes_5] was reduced to target ca. 0.3 wt % Au (full consumption of [Au_5Mes_5] is noted). A solution of [Au_5Mes_5] (1.0 mg, 0.004 mmol [Au_5Mes_5]/g TiO_2) in toluene (5 mL) was contacted with $TiO_{2\text{-}(120)}$ (171 mg) at room temperature, affording **3**.

Preparation of ***1-H$_2$****,* ***2-H$_2$****, and* ***3-H$_2$****.* The materials **1**, **2**, and **3** were treated under flowing H_2 (60 mL/min H_2 for 12 h at 300 °C, 0.5 °/min ramp) to afford a dark gray powder, **1-H$_2$**, **2-H$_2$**, and **3-H$_2$**.

Quantification of the Formation of Mesitylene. $TiO_{2\text{-}(120)}$ (10−20 mg) samples were placed in contact with a quantity of [Au_5Mes_5] corresponding the appropriate loadings for **1**, **2**, and **3** dissolved in ca. 1 mL of C_6D_6. The reaction was allowed to proceed as described above for the preparation of **1**−**3**. After 4 h under stirring at room temperature, the supernatant is separated via pipetting and the solid washed once with ca. 0.5 mL of C_6D_6, and all solutions were combined. Quantitative ^{1}H NMR using ferrocene as an internal standard was used to quantify mesitylene: 0.52 μmol mesitylene produced (0.34 μmol [Au_5Mes_5] consumed), 0.25 μmol (0.15 μmol [Au_5Mes_5] consumed), and 0.10 μmol (0.05 μmol [Au_5Mes_5] consumed) for **1**, **2**, and **3**, respectively.

NMR Characterization of Methanol Oxidation. A 2.9 mg sample of catalyst **2** was mixed with 1.08 mL of D_2O and 0.12 mL of $^{13}CH_3OH$ (Sigma-Aldrich). In a comparison to photocatalytic tests, excess catalyst was used due to a small scale of reaction and difficulty to accurately weight such small masses. A magnetic stir bar was inserted into the tube for agitation during the photocatalysis experiment. The sample was exposed to the same UV lamp used for the photocatalytic studies, with a cooling water bath around it to prevent overheating. Gas bubbles and H_2 were observed to form via GC. Photocatalysis was carried out under exclusion of air. The following standards used for NMR peak assignments were validated using HMBC ^{1}H−^{13}C NMR (solvent D_2O): formic acid (HCOOH), ^{13}C δ = 165 ppm, ^{1}H δ = 8.15 ppm; methyl formate ($HCOOCH_3$), ^{13}C δ = 167, 51.4 ppm, ^{1}H δ = 3.16, 3.78 ppm; methylene glycol (hydrated formaldehyde) ($CH_2(OH)_2$), ^{13}C δ = 81.7 ppm, ^{1}H δ = 4.19, 3.34 ppm; dimethoxymethane ($CH_2(OCH_3)_2$), ^{13}C δ = 96.8, 54.8 ppm, ^{1}H δ = 4.64, 3.38 ppm; methoxymethanol ($CH_2(OH)(OCH_3)$), formed by mixing an equimolar aqueous solution of formaldehye and methanol at room temperature for 19 h)), ^{13}C δ = 90.1, 55.2 ppm, ^{1}H δ = 4.72, 3.38 ppm.

Investigation of Photocatalytic Activity. The photoreactor consisting of a 500 mL jacketed reactor with a 220 mm jacketed quartz immersion well was purchased from Ace Glass, Inc. A quartz mercury low pressure UV arc lamp (450 W, Ace Glass, Inc.) was used to illuminate the photocatalysts. The energy output of the lamp after passing through a quartz cooling jacket with ca. 5 mm deionized water flowing was measured to be 190 mW/cm^2 using a Thorlabs PM100 optical power and energy meter. All joints of the reactor were lubricated with fluorinated grease (Krytox LVP, Dupont), as other greases are observed to decompose and leach H_2 under UV illumination. H_2 production was monitored using a micro-gas-chromatograph (490 Micro GC, Agilent Technologies, AG) with a 1 m CP-COX column used to separate H_2 from O_2. An oil filled bubbler was used to prevent backflow of ambient air into either the micro-GC or the reactor. Photocatalytic tests were performed under a flow (26 mL/min) of N_2, with a T junction going to the microGC allowing online sampling of the gases evolved. Photocatalysis was performed within a sealed (nonreflective) light-tight enclosure, and the reactor and UV lamp were cooled with 20 °C cooling water mantle. Agitation was provided via a Teflon stir bar spinning at 255 rpm. Prior to starting photocatalysis, the reactor was filled with a 10 vol % mixture of CH_3OH and H_2O, and degassed under dynamic vacuum (ca. 20 mbar) for 30 min, followed by deaeration with bubbling N_2 (26 mL/min) for 1 h. The catalyst (14.7 mg for **1**, 13.8 mg for **1-H$_2$**, 15.3 mg for **2**, 16.6

DOI: 10.1021/acs.inorgchem.6b00341
Inorg. Chem. XXXX, XXX, XXX−XXX

mg for **2-H$_2$**, 17.6 mg for **3**, 13.8 mg for **3-H$_2$**, 23.1 mg for **4**, and 18.7 mg for TiO$_{2\text{-}(120)}$) was then added under a flow of N_2, and deaerated with bubbling N_2 for 1 h more. Examination of overall water splitting was conducted in an identical matter except only pure H_2O was used. Oxygen production could not be quantified because of its absorption in degassed water.

GC analysis of the gas stream is conducted to verify that no oxygen is present in the outlet stream. NMR analysis of the reaction solution, following either the standard deaeration procedure or 24 h exposure to UV light and 26 mL/min N_2 bubbling without any photocatalyst, shows minimal loss of methanol. During photocatalysis, the micro-GC is programmed to sample the outlet gas stream on regular intervals, and the UV light is turned on at the same moment of the first GC sample. Once photocatalysis begins the reactor enclosure is not opened, and gas production is regularly monitored. Quantification of the H_2 production is done via TCD, which is calibrated prior to use. H_2 production is calculated with the following entities: v = volumetric flow rate (mL/min), c = concentration (vol %), n = molar flow rate (mol/min). Known quantities follow: v_{N2} (N_2 flow rate, 26 mL/min) and c_{H2} (concentration of H_2 measured by TCD, vol %), P = atmospheric pressure, 1.01 bar, T = 300 K.

The route for calculating volumetric H_2 flow follows:

$$v_{H2}(\text{mL/min}) = v_{N2} \times c_{H2}$$

Converting volumetric H_2 flow to molar H_2 flow using the ideal gas law

$$n_{H2}(\text{mol/min}) = \frac{Pv_{H2}}{RT}$$

This number is then either divided by the moles of Au present in the catalyst used, or by the mass of catalyst used.

Schematic Representation of the Experimental Setup. We show a representation of the experiment, although some items are not pictures: light tight box for photoreactor when UV light is illuminated, and jacket for cooling water for both lamp holder and photoreactor.

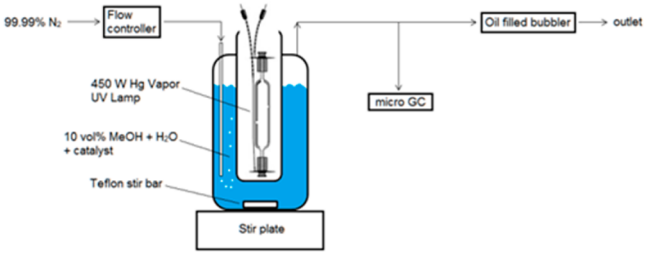

RESULTS AND DISCUSSION

Synthesis and Characterization of Au-TiO$_2$. Contacting an excess of [Au$_5$Mes$_5$] (4 Au/nm^2 TiO$_2$) on Evonik P25 TiO$_2$ partially dehydroxylated at 120 °C (TiO$_{2\text{-}(120)}$) affords a gray solid, **1**. Transmission electron microscopy (TEM) on this sample shows the presence of particles with a 0.9 nm average particle size, but with a noticeable tail of nanoparticles larger than 3 nm (Figure 1). Alternative modes of activation of the titania support (e.g., higher temperatures of dehydroxylation, cooling under N_2 or vacuum) lead to less reproducible gold deposition, yielding in particular larger particles and broader particle size distribution, indicating that surface state and the level of dehydroxylation of titania are important parameters.

^{1}H NMR of the supernatant confirms that [Au$_5$Mes$_5$] is partially consumed, corresponding to a deposition of ca. 3 wt % of Au on TiO$_2$ (see Supporting Information for details), consistent with 2.4 wt % loading determined by elemental analysis (Table 1). NMR of the filtrate after reaction reveals that approximately 1.4 equiv of mesitylene is released per [Au$_5$Mes$_5$] consumed upon contact with titania.

Table 1. Au-TiO$_2$ Synthesis Conditions and Effect on Au Loading and Nanoparticle Size

	targeted Au/nm^2[a]	Au wt %[b]	C/Au[c]	NP size[d] (nm)
1	4	2.4	8.5	0.9 ± 0.1
1-H$_2$[e]		2.4	*f*	0.9 ± 0.06
2	0.5	0.9	9.3	0.7 ± 0.05
2-H$_2$[e]		0.9	*f*	0.8 ± 0.04
3	0.2	0.3	*f*	0.6 ± 0.05
3-H$_2$[e]		0.3	*f*	0.8 ± 0.06
4		1.2	*f*	1.7 ± 0.08

[a]Targeted surface loading of Au atoms per nm^2 of TiO$_2$, calculated from the concentration of Au used. [b]Weight loading of Au on TiO$_2$, determined by elemental analysis (EA). [c]Atomic ratio of C/Au present on TiO$_2$, determined by EA. [d]Average particle size of Au, determined by TEM analysis, 95% confidence interval reported. [e]Prepared via a post-treatment under 10 mL/min H_2 flow at 300 °C (0.5 °C/min) for 10 h. [f]Amount of carbon present was too low (<0.2 wt %) for accurate EA.

We reasoned that the larger particles could arise via the growth of small nanoparticles from the excess of [Au$_5$Mes$_5$] present in solution during the deposition step. To limit this possibility, we used a default of [Au$_5$Mes$_5$] corresponding to 10 (0.9 wt %, **2**) and 5 (0.3 wt %, **3**) μmol [Au$_5$Mes$_5$] per g TiO$_2$ (0.5 and 0.2 Au/nm^2, respectively). From quantitative mass balance analysis of the filtrate by NMR, we observe that in both cases [Au$_5$Mes$_5$] is fully consumed, corresponding to the 0.9 and 0.3 wt % Au in **2** and **3**, respectively (Table 1). Similar to **1**, NMR spectra of the filtrates of **2** and **3** after reaction reveal that 1.7 and 2 equiv of mesitylene, respectively, are released per equiv of [Au$_5$Mes$_5$] consumed. TEM pictures of catalysts **2** and **3** reveal an average particle size of 0.7 nm for **2** and 0.6 nm for **3** and an elimination of the tail in the PSD (Figure S1), corresponding to ca. 15 atom clusters.[51]

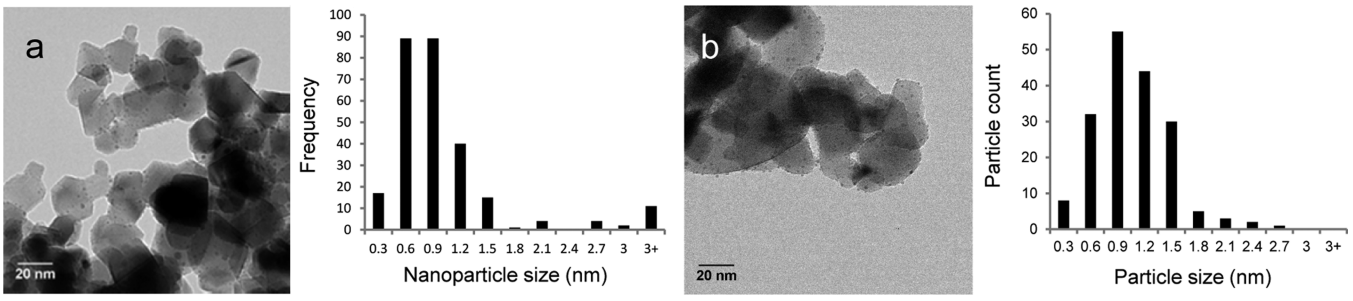

Figure 1. Representative TEM images (left) and particle size distributions (right) of (a) **1** and (b) **1-H$_2$**.

DOI: 10.1021/acs.inorgchem.6b00341
Inorg. Chem. XXXX, XXX, XXX−XXX

UV−vis DRS under inert atmosphere of **1** and **1-H$_2$** shows only a very weak plasmon resonance peak, probably associated with the very small particle size, which increases upon exposure to air (Figure S13).[52,53] IR spectroscopy after deposition shows the presence of stretching and bending (C−H) vibrations in the 3080−2800 and 1500−1350 cm^{-1} regions, respectively (Figure 2).

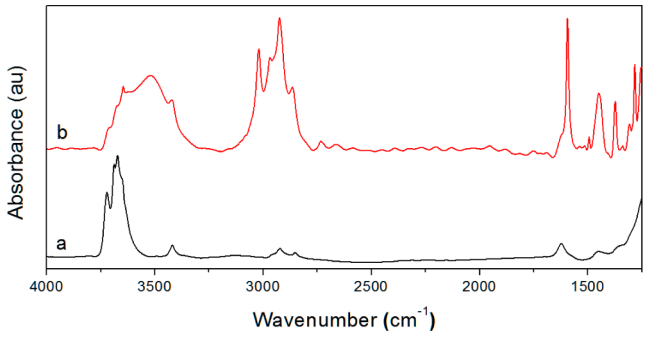

Figure 2. Transmission IR measurement of (a) partially dehydroxylated $TiO_{2\text{-}(120)}$ and (b) $TiO_{2\text{-}(120)}$ contacted with $[Au_5Mes_5]$ (**1**). Spectra are not normalized.

Due to the lack of post-treatment performed on **1**−**3**, significant amounts of organic moieties remain adsorbed on the surface, as evidenced by IR and EA with a C/Au ratio of ca. 9 (Table 1). In a comparison of the IR spectra of **1** to $[Au_5Mes_5]$ and $[Au_5Mes_5]$ physisorbed onto SiO_2,[50] the spectra of **1** is slightly shifted and distorted, consistent with the presence of adsorbed mesityl containing species in a different chemical environment than in $[Au_5Mes_5]$ (Figure S2). The observation of mesitylene (ca. 1.5−2 mol per mol $[Au_5Mes_5]$) in the filtrate and its ability to adsorb on oxide supports[50] suggest that it can still be adsorbed at the surface along with chemisorbed $[Au_5Mes_5]$. The consumption of −OH and $-OH_2$ bands of $TiO_{2\text{-}(120)}$ (3600−3700 cm^{-1}) following deposition indicates that deposition occurs primarily via reaction with surface hydroxyl groups of TiO_2 (Figure 2). In addition, the disappearance of the peak in the IR spectra of $TiO_{2\text{-}(120)}$ at 1624 cm^{-1} corresponding to adsorbed water[54] suggests that nanoparticles are formed via the controlled hydrolysis of $[Au_5Mes_5]$ with the adsorbed water, yielding unstable Au_xO_y clusters, which disproportionate to give Au(0) clusters.[55] This is supported by the lack of Au nanoparticle formation on TiO_2 calcined at 450 °C or dehydroxylated silica that does not contain adsorbed H_2O.[50] From this analysis and the subnanometer Au particles observed by TEM, we can hypothesize that Au is present on the surface as either mesityl capped Au nanoparticles and/or chemisorbed $[Au_5Mes_5]$.

To elucidate this further, we turned to XANES, which shows the presence of a mixture of gold(0) and gold(I) species in **1**, using Au^0-SiO_2 and $[Au^I_5Mes_5]$, as references (Figures S3−5, Supporting Information).[50] In addition, STEM-EDX has a detectable Au EDX signal in regions without observable Au nanoparticles, suggesting the presence of chemisorbed Au species not present as nanoparticles. XANES and STEM-EDX, combined with the TEM, EA, and IR, suggest that chemisorbed $[Au_5Mes_5]$ surface species coexists on the surface with Au particles (bare or mesityl capped).

To remove remaining mesitylene and mesityl ligands, **1**, **2**, and **3** were treated under a flow of H_2 at 300 °C for 10 h, forming **1-H$_2$**, **2-H$_2$**, **3-H$_2$**, respectively. After this step, no C−H stretches are observed in the 2900 cm^{-1} region of the IR (Figure S8), and only trace amounts of carbon (<0.2 wt %) can be detected by elemental analysis (Table 1). XANES shows the presence of only gold(0) species (Figure S5). TEM indicates a minor increase in mean particle size by 0−0.2 nm, but also an

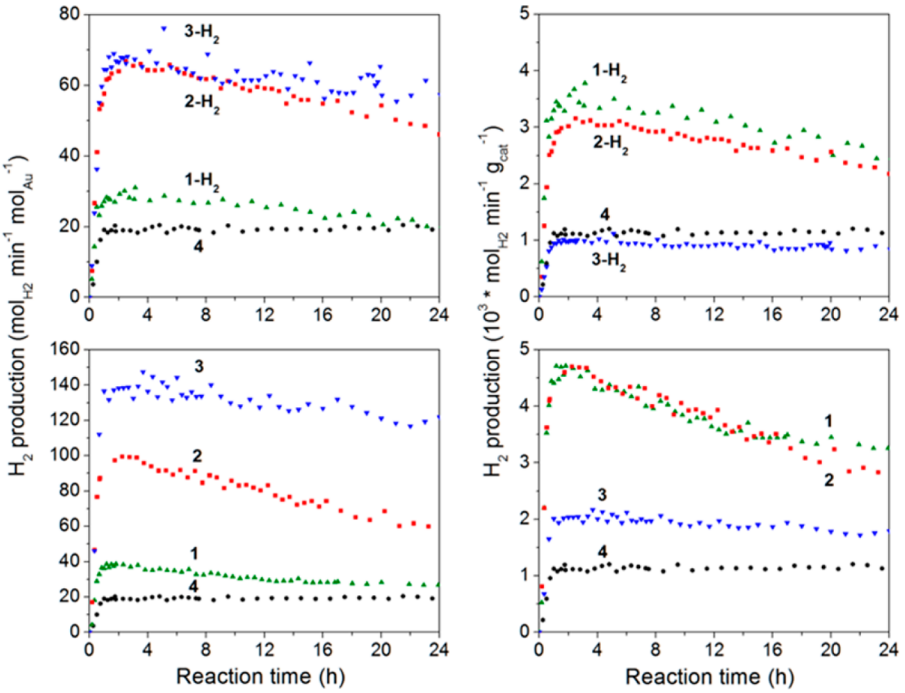

Figure 3. H_2 production of **4** and the H_2-treated catalysts (top) and as-synthesized catalysts (bottom) normalized to the amount of Au present in the sample (left), and the mass of catalyst (right). $TiO_{2\text{-}(120)}$ has been omitted for clarity. Reaction consists of a deaerated 10 vol % mixture of CH_3OH + H_2O with 15−25 mg of catalyst, exposed to a 450 W Hg vapor UV light under a 26 mL/min N_2 flow.

DOI: 10.1021/acs.inorgchem.6b00341
Inorg. Chem. XXXX, XXX, XXX−XXX

increase in nanoparticle surface density compared to the as-synthesized catalysts (Figure S1) and[56] the disappearance of the larger particle (>3 nm) in the PSD of **1** (Figure 1). This result is consistent with a redispersion of Au after reduction as recently observed on various supports.[50,57] This increase in particle density is consistent with the presence of chemisorbed $[Au_5Mes_5]$ species prior to the treatment under H_2, which are then converted into additional Au nanoparticles.

Overall, the deposition of $[Au_5Mes_5]$ onto TiO_2 followed by a mild treatment under H_2 allows for a simple and robust synthesis for subnanometer Au particles supported on TiO_2. In view of the ease of preparation of $[Au_5Mes_5]$ in g-scale, this approach provides a scalable route to a narrow particle size distribution of Au particles which are in the range of the smallest reported Au nanoparticles supported on TiO_2 to our knowledge.[39,58−64]

Photocatalytic Performance of Au-TiO_2. Having synthesized these subnanometer Au-TiO_2 catalysts, we investigated their photocatalytic performance for methanol-assisted hydrogen evolution (Figure 3). To allow long-term catalyst testing we operated our reactor with a continuous flow of N_2 bubbling through the reactor during photocatalysis, and quantified the production of H_2 by gas chromatography. Since differences such as lamp power, photocell design, and catalyst loading can yield significantly different activities, commercial AUROlite 1.2 wt % Au-TiO_2 (**4**) was studied as a reference catalyst.[65] XRD shows **4** is a mixture of anatase and rutile identical to P25, and the support particle size calculated by the Debye−Scherrer equation of **4** is 27 nm, confirming that the support is P25 TiO_2. The average Au particle size from TEM was measured to be 1.7 nm (Table 1, Figure S9), similar to other published catalysts.[39,40] To facilitate photocatalysis, methanol was selected as an electron donor, as commonly described in literature.[5,66]

With similar weight loading and identical support of **2-H_2** and **4**, one can make a direct comparison and show that the peak activity of **2-H_2**, both per mol_{Au} and g_{cat}, is 3-fold higher than that for **4**. The most active catalysts are **3-H_2** and **1-H_2**, per mol_{Au} and per g_{cat}, respectively. NMR analysis of the reaction mixtures after 69 h of photocatalysis shows the formation of $CH_2(OH)_2$, $CH_2(OH)(OCH_3)$, HCOOH, $HCOOCH_3$, and dissolved CO_2 (Table S3), consistent with the photooxidation of methanol (reactions 1−13 in Supporting Information).[67−69] This data confirms that methanol acts as a scavenging agent for oxidants during photocatalysis.

Since TiO_2 photocatalysts are very efficient at degrading organic molecules under UV light,[70] we suspected that the presence of mesityl groups on the surface of the as-synthesized Au nanoparticles would not significantly hinder catalytic performance, and tested the performance of **1**, **2**, and **3** (Figure 3). In fact, all the as-synthesized catalysts **1**, **2**, and **3** display significantly greater activity than their H_2-treated counterparts, **1-H_2**, **2-H_2**, and **3-H_2**, respectively. Finally, although activities are higher, the trends in activity of the as-synthesized catalysts are the same as those previously noted. Since the average observable particle sizes of the H_2-treated and as-synthesized catalysts are similar, the increase of photocatalytic activity is associated with the presence of chemisorbed $[Au_5Mes_5]$ prior to photocatalysis and probably originates from the in situ formation of small Au clusters from the decomposition of $[Au_5Mes_5]$ under photocatalysis conditions.

To confirm that hydrogen evolution occurs even in the absence of methanol, photocatalytic hydrogen evolution was conducted on **2** and **4** in pure water. Although the catalysts experienced rapid deactivation similar to benchmark catalyst and previous studies,[31] **2** produces as much as ca. 3−4 times more hydrogen than **4** (Figure S12), but it was not possible to quantify the O_2 produced with our experimental setup.

A summary of the total amount of hydrogen produced for each catalyst after 100 h reaction time is presented in Figure 4.

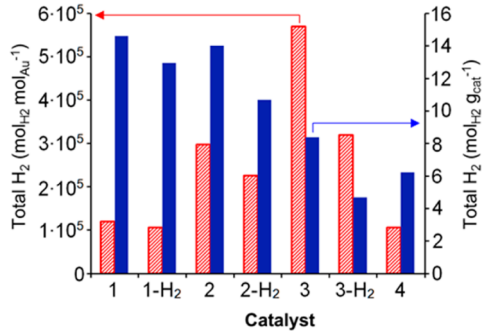

Figure 4. Total H_2 generated after 100 h reaction time per mol_{Au} (left) and per g_{cat} (right). Total H_2 generation calculated by numerical integration of the curves in Figure S10.

We observe that the same trends hold as with the peak activity (Figure 4, Table S1): H_2-treated catalysts produce less H_2 than the as-synthesized catalysts, and H_2 generation per mol_{Au} basis increases with decreasing weight loading, with the reverse occurring per g_{cat}. By comparison, the bare support, $TiO_{2\text{-}(120)}$, has negligible activity.

In agreement with previous studies showing the benefit of reducing particle size,[47,71−75] these TiO_2-supported subnanometer Au particles also display some of the best reported photocatalytic activities.[5,66,76] This exceptionally high activity is most likely due to the presence of subnanometer Au particles with a relatively narrow particle size distribution. Although further work is required to elucidate the mechanism by which these subnanometer particles enhance activity, the high activity of subnanometer particles parallels what has been found for a range of metals (Cu, Ag, Pt, Au) and reactions (propylene oxidation, hydrogen generation, CO oxidation), in particular for Au, which is typically inactive as a bulk metal.[77−82]

Deactivation. Despite their high activity, these subnanometer Au-TiO_2 catalysts undergo significant deactivation (Figure 3, Table 2). In all catalysts, the sizes of the Au particle increase, by 1.1−1.3 nm for **1**, **2**, and **3** and the 0.7−0.9 nm for **1-H_2**, **2-H_2**, and **3-H_2**. This size increase parallels the level of deactivation of 63−68% versus 35−59% observed for the as-synthesized and H_2-treated catalysts, respectively (Tables 1 and 2), supporting sintering as a deactivation mechanism. This is further evidenced by the lower deactivation of **3-H_2**, which has lower weight loading (0.3 wt %) and particle density. It is noteworthy that Au sintering requires both water and UV light (a catalyst exposed to only one of them does not suffer from sintering). This suggests that Au sintering probably results from radical species formed in solution or at the interface between the solid and the solution, and not only electron−hole pairs.

In addition, examining the photocatalytic performance of $TiO_{2\text{-}(120)}$ indicates that even the bare support experiences deactivation, losing 40% of its activity after 60 h of photocatalysis, which suggests the participation of alternative deactivation pathway. Previous studies have found similar deactivation of bare TiO_2, and have correlated this to corrosion of the TiO_2 surface by photogenerated holes.[83,84] In fact,

DOI: 10.1021/acs.inorgchem.6b00341
Inorg. Chem. XXXX, XXX, XXX−XXX

Table 2. Summary of Deactivation and Sintering During Photocatalysis

	deactivation[a] (%)	d_{NP} before photocat[b] (nm)	d_{NP} after photocat[c] (nm)	Δd_{NP}[d] (nm)
1	68	0.9 ± 0.1	2.0 ± 0.1	1.1
1-H$_2$	59	0.9 ± 0.06	1.8 ± 0.08	0.9
2	69	0.7 ± 0.05	1.9 ± 0.1	1.2
2-H$_2$	63	0.8 ± 0.04	1.7 ± 0.07	0.9
3	54	0.6 ± 0.05	1.9 ± 0.1	1.3
3-H$_2$	35	0.8 ± 0.06	1.5 ± 0.1	0.7
4	30	1.7 ± 0.08	1.9 ± 0.1	0.2

[a]Deactivation calculated by percentage change between peak activity and averaged photocatalytic activity from 98 to 100 h. [b]Average Au particle size before reaction, taken from Table 1. [c]Average Au particle size after 100 h reaction, with representative TEM images and PSD shown in Figure S11. [d](Final Au particle size) − (initial Au particle size).

investigation of Au-TiO$_2$ catalysts after photocatalysis by TEM shows the formation of an amorphous layer after reaction which encapsulates the material, which could be related to this phenomenon (Figure S11 and Figure S18). TEM studies of bare TiO$_2$ after photocatalysis in pure water also showed layer formation (Figure S18). This layer is likely a hydroxide layer on top of TiO$_2$, which probably forms by leaching−redeposition of TiO$_2$ under water splitting conditions.[67,85,86]

CONCLUSIONS

Subnanometer Au particles with a narrow particle size distribution were prepared with up to 2 wt % loading through a two-step process involving the reaction of [Au$_5$Mes$_5$] with partially dehydroxylated TiO$_2$ at 120 °C, followed by a mild treatment under H$_2$. Characterization of the material via EA, IR, and XANES and STEM-EDX shows that the surface of TiO$_2$ after the deposition step is already decorated with gold(0) nanoparticles along with residual chemisorbed [Au$_5$Mes$_5$] and/or gold(0) nanoparticles stabilized by mesityl ligands. The formation of Au(0) presumably arises from the controlled hydrolysis of [Au$_5$Mes$_5$], with water chemisorbed on TiO$_2$, into Au$_x$O$_y$, which is then converted into Au(0) particles. Post-treatment under H$_2$ efficiently removes the organic groups and converts residual [Au$_5$Mes$_5$] to selectively afford subnanometer narrowly dispersed metallic Au particles, thus providing a simple synthesis route to subnanometer Au particles on TiO$_2$. These H$_2$-treated Au nanoparticles display high activity in H$_2$ evolution, showing that lowering the nanoparticle size into the subnanometer range is a viable strategy to significantly improve photocatalytic performance. The as-synthesized Au-TiO$_2$ catalysts display even higher activity, demonstrating the potential of smaller Au clusters generated from chemisorbed [Au$_5$Mes$_5$] for photocatalytic hydrogen evolution. In addition, deactivation has been shown to be related to both sintering and the growth of an amorphous layer around the catalytic particle. Overall, the ease of transposition of this approach to other structured semiconductors and the evidence for deactivation pathways pave the way for a more rational improvement of the efficiency (activity and stability) of photocatalysts through a better tuning of the metal cocatalysts.

ASSOCIATED CONTENT

Supporting Information

The Supporting Information is available free of charge on the ACS Publications website at DOI: 10.1021/acs.inorgchem.6b00341.

Experimental details, additional TEM images and particle size distributions before and after photocatalysis, IR spectra of additional compounds, XANES and STEM-EDX analysis, XRD and TEM characterization of **4**, photocatalytic data after 140 h reaction time, and tables summarizing photocatalytic performance (PDF)

AUTHOR INFORMATION

Corresponding Author

*E-mail: ccoperet@ethz.ch.

Author Contributions

The manuscript was written through contributions of all authors. All authors have given approval to the final version of the manuscript.

Notes

The authors declare no competing financial interest.

ACKNOWLEDGMENTS

We acknowledge the Paul Scherrer Institut, in Villigen, Switzerland, for provision of synchrotron radiation beamtime at the SuperXAS beamline of the SLS and would like to thank Dr. Olga Safonova and Dr. Maarten Nachtegaal for their assistance. We are grateful to ScopeM for the use of their microscopy facilities and Mr. Dmitry Lebedev for assistance with XRD spectroscopy and analysis. G.S. would like to thank the Swiss National Science Foundation (SNF 200021_137691/1 and SNF 200020_159801) for funding. V.M. was supported by an ETH fellowship (cofunded ETH Zürich-Marie Curie action for people, FEL-08-12-2).

REFERENCES

(1) Fujishima, A.; Honda, K. *Nature* **1972**, *238*, 37.
(2) Asahi, R.; Morikawa, T.; Ohwaki, T.; Aoki, K.; Taga, Y. *Science* **2001**, *293*, 269.
(3) Hashimoto, K.; Irie, H.; Fujishima, A. *Jpn. J. Appl. Phys.* **2005**, *44*, 8269.
(4) Yoshimura, J.; Ebina, Y.; Kondo, J.; Domen, K.; Tanaka, A. *J. Phys. Chem.* **1993**, *97*, 1970.
(5) Kudo, A.; Miseki, Y. *Chem. Soc. Rev.* **2009**, *38*, 253.
(6) Niishiro, R.; Tanaka, S.; Kudo, A. *Appl. Catal., B* **2014**, *150−151*, 187.
(7) Baba, R.; Nakabayashi, S.; Fujishima, A.; Honda, K. *J. Phys. Chem.* **1985**, *89*, 1902.
(8) Townsend, T. K.; Browning, N. D.; Osterloh, F. E. *ACS Nano* **2012**, *6*, 7420.
(9) Domen, K.; Naito, S.; Soma, M.; Onishi, T.; Tamaru, K. *J. Chem. Soc., Chem. Commun.* **1980**, 543.
(10) Ebina, Y.; Tanaka, A.; Kondo, J. N.; Domen, K. *Chem. Mater.* **1996**, *8*, 2534.
(11) Hitoki, G.; Ishikawa, A.; Takata, T.; Kondo, J. N.; Hara, M.; Domen, K. *Chem. Lett.* **2002**, *31*, 736.
(12) Wagner, F. T.; Somorjai, G. A. *Nature* **1980**, *285*, 559.

DOI: 10.1021/acs.inorgchem.6b00341
Inorg. Chem. XXXX, XXX, XXX−XXX

(13) Ran, J.; Zhang, J.; Yu, J.; Jaroniec, M.; Qiao, S. Z. *Chem. Soc. Rev.* **2014**, *43*, 7787.
(14) Ma, Y.; Wang, X.; Jia, Y.; Chen, X.; Han, H.; Li, C. *Chem. Rev.* **2014**, *114*, 9987.
(15) Bian, Z.; Tachikawa, T.; Zhang, P.; Fujitsuka, M.; Majima, T. *J. Am. Chem. Soc.* **2014**, *136*, 458.
(16) Zhang, Z.; Wang, C.-C.; Zakaria, R.; Ying, J. Y. *J. Phys. Chem. B* **1998**, *102*, 10871.
(17) Su, R.; Tiruvalam, R.; Logsdail, A. J.; He, Q.; Downing, C. A.; Jensen, M. T.; Dimitratos, N.; Kesavan, L.; Wells, P. P.; Bechstein, R.; Jensen, H. H.; Wendt, S.; Catlow, C. R. A.; Kiely, C. J.; Hutchings, G. J.; Besenbacher, F. *ACS Nano* **2014**, *8*, 3490.
(18) Tsukamoto, D.; Shiraishi, Y.; Sugano, Y.; Ichikawa, S.; Tanaka, S.; Hirai, T. *J. Am. Chem. Soc.* **2012**, *134*, 6309.
(19) Murdoch, M.; Waterhouse, G. I. N.; Nadeem, M. A.; Metson, J. B.; Keane, M. A.; Howe, R. F.; Llorca, J.; Idriss, H. *Nat. Chem.* **2011**, *3*, 489.
(20) Domen, K.; Ebina, Y.; Sekine, T.; Tanaka, A.; Kondo, J.; Hirose, C. *Catal. Today* **1993**, *16*, 479.
(21) Wagner, F. T.; Somorjai, G. A. *J. Am. Chem. Soc.* **1980**, *102*, 5494.
(22) Subramanian, V.; Wolf, E.; Kamat, P. V. *J. Phys. Chem. B* **2001**, *105*, 11439.
(23) Kato, H.; Asakura, K.; Kudo, A. *J. Am. Chem. Soc.* **2003**, *125*, 3082.
(24) Ma, S. S. K.; Hisatomi, T.; Maeda, K.; Moriya, Y.; Domen, K. *J. Am. Chem. Soc.* **2012**, *134*, 19993.
(25) Zou, Z.; Ye, J.; Sayama, K.; Arakawa, H. *Nature* **2001**, *414*, 625.
(26) Chen, X.; Liu, L.; Yu, P. Y.; Mao, S. S. *Science* **2011**, *331*, 746.
(27) Zhang, Y.; Zhang, J.; Xu, Q.; Yan, S.; Zhao, S.; Luo, G.; Li, C. *Mater. Res. Bull.* **2014**, *53*, 107.
(28) Domen, K.; Kondo, J. N.; Hara, M.; Takata, T. *Bull. Chem. Soc. Jpn.* **2000**, *73*, 1307.
(29) Primo, A.; Corma, A.; Garcia, H. *Phys. Chem. Chem. Phys.* **2011**, *13*, 886.
(30) Bamwenda, G. R.; Tsubota, S.; Nakamura, T.; Haruta, M. *J. Photochem. Photobiol., A* **1995**, *89*, 177.
(31) Rosseler, O.; Shankar, M. V.; Du, M. K.-L.; Schmidlin, L.; Keller, N.; Keller, V. *J. Catal.* **2010**, *269*, 179.
(32) Iwase, A.; Kato, H.; Kudo, A. *Catal. Lett.* **2006**, *108*, 7.
(33) Gomes Silva, C.; Juárez, R.; Marino, T.; Molinari, R.; García, H. *J. Am. Chem. Soc.* **2011**, *133*, 595.
(34) Serra, M.; Albero, J.; García, H. *ChemPhysChem* **2015**, *16*, 1842.
(35) Priebe, J. B.; Karnahl, M.; Junge, H.; Beller, M.; Hollmann, D.; Brückner, A. *Angew. Chem., Int. Ed.* **2013**, *52*, 11420.
(36) Liu, L.; Li, P.; Adisak, B.; Ouyang, S.; Umezawa, N.; Ye, J.; Kodiyath, R.; Tanabe, T.; Ramesh, G. V.; Ueda, S.; Abe, H. *J. Mater. Chem. A* **2014**, *2*, 9875.
(37) Naldoni, A.; Riboni, F.; Marelli, M.; Bossola, F.; Ulisse, G.; Di Carlo, A.; Pis, I.; Nappini, S.; Malvestuto, M.; Dozzi, M. V.; Psaro, R.; Selli, E.; Dal Santo, V. *Catal. Sci. Technol.* **2016**, DOI: 10.1039/C5CY01736J.
(38) Naldoni, A.; Fabbri, F.; Altomare, M.; Marelli, M.; Psaro, R.; Selli, E.; Salviati, G.; Dal Santo, V. *Phys. Chem. Chem. Phys.* **2015**, *17*, 4864.
(39) Bamwenda, G. R.; Tsubota, S.; Nakamura, T.; Haruta, M. *Catal. Lett.* **1997**, *44*, 83.
(40) Moreau, F.; Bond, G. C.; Taylor, A. O. *J. Catal.* **2005**, *231*, 105.
(41) Chan, S. C.; Barteau, M. A. *Langmuir* **2005**, *21*, 5588.
(42) Cunningham, D.; Tsubota, S.; Kamijo, N.; Haruta, M. *Res. Chem. Intermed.* **1993**, *19*, 1.
(43) Gong, X.-Q.; Selloni, A.; Dulub, O.; Jacobson, P.; Diebold, U. *J. Am. Chem. Soc.* **2008**, *130*, 370.
(44) Diebold, U. *Surf. Sci. Rep.* **2003**, *48*, 53.
(45) Louis, C.; Pluchery, O. *Gold Nanoparticles for Physics, Chemistry and Biology*; World Scientific, 2012.
(46) de Jong, K. P. *Synthesis of Solid Catalysts*; John Wiley & Sons, 2009.
(47) Subramanian, V.; Wolf, E. E.; Kamat, P. V. *J. Am. Chem. Soc.* **2004**, *126*, 4943.
(48) Valden, M.; Lai, X.; Goodman, D. W. *Science* **1998**, *281*, 1647.
(49) Arabatzis, I. M.; Stergiopoulos, T.; Andreeva, D.; Kitova, S.; Neophytides, S. G.; Falaras, P. *J. Catal.* **2003**, *220*, 127.
(50) Siddiqi, G.; Mougel, V.; Coperet, C. *Dalton Trans.* **2015**, *44*, 14349.
(51) Jentys, A. *Phys. Chem. Chem. Phys.* **1999**, *1*, 4059.
(52) Njoki, P. N.; Lim, I. I. S.; Mott, D.; Park, H.-Y.; Khan, B.; Mishra, S.; Sujakumar, R.; Luo, J.; Zhong, C.-J. *J. Phys. Chem. C* **2007**, *111*, 14664.
(53) Amendola, V.; Meneghetti, M. *J. Phys. Chem. C* **2009**, *113*, 4277.
(54) Arrouvel, C.; Digne, M.; Breysse, M.; Toulhoat, H.; Raybaud, P. *J. Catal.* **2004**, *222*, 152.
(55) Tsai, H.; Hu, E.; Perng, K.; Chen, M.; Wu, J.-C.; Chang, Y.-S. *Surf. Sci.* **2003**, *537*, L447.
(56) Nanoparticle density calculated by counting the number of observable Au particles per unit area of the TEM picture.
(57) Romero-Sarria, F.; Martínez T, L. M.; Centeno, M. A.; Odriozola, J. A. *J. Phys. Chem. C* **2007**, *111*, 14469.
(58) Guzman, J.; Kuba, S.; Fierro-Gonzalez, J.; Gates, B. *Catal. Lett.* **2004**, *95*, 77.
(59) Aguilar-Guerrero, V.; Gates, B. *Catal. Lett.* **2009**, *130*, 108.
(60) Zanella, R.; Giorgio, S.; Henry, C. R.; Louis, C. *J. Phys. Chem. B* **2002**, *106*, 7634.
(61) Kilmartin, J.; Sarip, R.; Grau-Crespo, R.; Di Tommaso, D.; Hogarth, G.; Prestipino, C.; Sankar, G. *ACS Catal.* **2012**, *2*, 957.
(62) Fierro-Gonzalez, J. C.; Gates, B. C. *J. Phys. Chem. B* **2005**, *109*, 7275.
(63) Grunwaldt, J.-D.; Kiener, C.; Wögerbauer, C.; Baiker, A. *J. Catal.* **1999**, *181*, 223.
(64) Zheng, N.; Stucky, G. D. *J. Am. Chem. Soc.* **2006**, *128*, 14278.
(65) Reference catalyst **4** was chosen for its ease of commercial availability via Strem, Inc. to encourage duplication of our results.
(66) Chen, X.; Shen, S.; Guo, L.; Mao, S. S. *Chem. Rev.* **2010**, *110*, 6503.
(67) Chiarello, G. L.; Ferri, D.; Selli, E. *J. Catal.* **2011**, *280*, 168.
(68) Bahnemann, D. W.; Hilgendorff, M.; Memming, R. *J. Phys. Chem. B* **1997**, *101*, 4265.
(69) Villarreal, T. L.; Gómez, R.; Neumann-Spallart, M.; Alonso-Vante, N.; Salvador, P. *J. Phys. Chem. B* **2004**, *108*, 15172.
(70) Zhao, W.; Ma, W.; Chen, C.; Zhao, J.; Shuai, Z. *J. Am. Chem. Soc.* **2004**, *126*, 4782.
(71) Wu, G.; Chen, T.; Su, W.; Zhou, G.; Zong, X.; Lei, Z.; Li, C. *Int. J. Hydrogen Energy* **2008**, *33*, 1243.
(72) Kaur, R.; Pal, B. *J. Mol. Catal. A: Chem.* **2012**, *355*, 39.
(73) Su, R.; Tiruvalam, R.; He, Q.; Dimitratos, N.; Kesavan, L.; Hammond, C.; Lopez-Sanchez, J. A.; Bechstein, R.; Kiely, C. J.; Hutchings, G. J.; Besenbacher, F. *ACS Nano* **2012**, *6*, 6284.
(74) Li, J.; Zeng, H. C. *Angew. Chem., Int. Ed.* **2005**, *44*, 4342.
(75) Iliev, V.; Tomova, D.; Bilyarska, L.; Tyuliev, G. *J. Mol. Catal. A: Chem.* **2007**, *263*, 32.
(76) For comparison of similar light sources (400−450 W Hg vapor UV lamp), tabulated values of photocatalytic hydrogen production of several highly cited studies using a similar light source are provided in Table S2.
(77) Lei, Y.; Mehmood, F.; Lee, S.; Greeley, J.; Lee, B.; Seifert, S.; Winans, R. E.; Elam, J. W.; Meyer, R. J.; Redfern, P. C.; Teschner, D.; Schlögl, R.; Pellin, M. J.; Curtiss, L. A.; Vajda, S. *Science* **2010**, *328*, 224.
(78) Wei, W.; Lu, Y.; Chen, W.; Chen, S. *J. Am. Chem. Soc.* **2011**, *133*, 2060.
(79) Berr, M.; Vaneski, A.; Susha, A. S.; Rodríguez-Fernández, J.; Döblinger, M.; Jäckel, F.; Rogach, A. L.; Feldmann, J. *Appl. Phys. Lett.* **2010**, *97*, 093108.
(80) Yang, X.-F.; Wang, A.; Qiao, B.; Li, J.; Liu, J.; Zhang, T. *Acc. Chem. Res.* **2013**, *46*, 1740.
(81) Gao, Y.; Shao, N.; Pei, Y.; Chen, Z.; Zeng, X. C. *ACS Nano* **2011**, *5*, 7818.

DOI: 10.1021/acs.inorgchem.6b00341
Inorg. Chem. XXXX, XXX, XXX−XXX

(82) Lee, S.; Molina, L. M.; López, M. J.; Alonso, J. A.; Hammer, B.; Lee, B.; Seifert, S.; Winans, R. E.; Elam, J. W.; Pellin, M. J.; Vajda, S. *Angew. Chem., Int. Ed.* **2009**, *48*, 1467.
(83) Imanishi, A.; Okamura, T.; Ohashi, N.; Nakamura, R.; Nakato, Y. *J. Am. Chem. Soc.* **2007**, *129*, 11569.
(84) Yang, Y.; Ling, Y.; Wang, G.; Liu, T.; Wang, F.; Zhai, T.; Tong, Y.; Li, Y. *Nano Lett.* **2015**, *15*, 7051.
(85) Oakton, E.; Siddiqi, G.; Fedorov, A.; Coperet, C. *New J. Chem.* **2016**, *40*, 217.
(86) Tao, W.-H.; Tsai, C.-H. *Sens. Actuators, B* **2002**, *81*, 237.

DOI: 10.1021/acs.inorgchem.6b00341
Inorg. Chem. XXXX, XXX, XXX−XXX